Image Edge Detection Using FHN-CNN Model Based on Reaction-Diffusion Equations within a Dynamical Systems Framework

Zhao Yang
Academic Affairs Office, Zibo Polytechnic University, Zibo, 255314, China
E-mail: zhaoyang_zyang@outlook.com

Keywords: dynamical system, reaction-diffusion equation, image processing, FHN, Cellular-NN, zuring spot

Received: August 12, 2025

With the advancement of imaging technology, images present diverse and highly complex characteristics, and the theory of dynamical systems has great potential in image processing due to its unique mathematical properties. Therefore, this study proposes an IPT based on the reaction-diffusion equation. This technique combines cellular neural networks with the reaction-diffusion equation within the framework of dynamical system theory. Specifically, by introducing the Laplacian operator, the membrane potential in the FitzHugh-Nagumo equation is correlated with the spatiotemporal dynamics of the recovery variable. A new type of image processing model is constructed by mapping to the dynamic evolution of locally coupled mesh cells in convolutional neural networks. The theoretical framework of the technology is further improved through the dynamic analysis of the Turing instability of the model and the gradient changes of the reaction-diffusion system. The results showed that in the performance testing of the research model, the Edge Preservation Index (EPI) was 0.89 and the Pratt's Figure of Merit (PFOM) was 0.95, which were higher than the comparison models, indicating excellent model performance. Meanwhile, the time cost for the new model to complete one detection was only 0.9 seconds, and there were only 2 iterations, which was significantly better than other models. Research has shown that the new model has higher computational efficiency and better real-time performance. This study provides new ideas and methods for image processing and helps to promote the development of image processing algorithms towards high efficiency and intelligence.

Povzetek: Predlagan reakcijsko-difuzijski model obdelave slik doseže boljšo ohranitev robov in hitrejše delovanje kot primerjalne metode.

1 Introduction

Early Image Processing Techniques (IPTs) were mainly used to improve image quality, such as image denoising and enhancing image contrast. The advancement of computer technology has led IPT to gradually enter the stage of digital image processing, placing higher demands on the real-time and precision of image processing [1]. To meet the needs of digital transformation, IPT's core algorithms have transitioned from manual algorithms and simple mathematical models to Deep Learning (DL) models [2]. Numerous scholars have conducted research on IPT. Zangana et al. explored the combination of edge detection and existing image processing methods, and summarized the advantages and limitations of existing edge detection methods. Advanced methods utilizing DL, fuzzy logic, and optimization algorithms have shown good results in improving edge detection accuracy [3-4]. Chen et al. proposed a DL-based post-processing method for magnetic resonance images. The processing steps included noise reduction, image artifact correction, and image resolution improvement. This method had a significant effect on improving image quality and correcting image artifacts [5]. Zhou et al. proposed an underwater image enhancement method based on multi-interval sub-histogram perspective equalization. This method extracted statistical features of the image, estimated the degree of feature drift in each region of the image, and achieved adaptive feature enhancement. The experiment showed that this method was significantly superior to existing methods in both qualitative and quantitative aspects [6]. Zhang et al. proposed an underwater image enhancement method based on weighted wavelet visual perception fusion to address the issue of degraded underwater image quality. This method integrated high-frequency and low-frequency components of images at different scales to obtain high-quality underwater images, which were superior to the latest methods in both qualitative and quantitative aspects [7]. Jiang et al. proposed a diffusion-based low-light image enhancement method to address long processing time and high computational resource consumption in image restoration using diffusion models. It introduced a high-frequency recovery module, achieving better fine-grained recovery and significantly improving efficiency compared to previous diffusion-based methods [8]. Arshaghi et al. proposed a method based on Convolutional Neural Network (CNN) for the problem of agricultural product defect identification. They studied

the classification of five potato diseases and conducted experiments using 5,000 images. The results showed that this method outperformed other existing methods in terms of the accuracy of defect classification [9].

Reaction Diffusion Equation (RDE) is a type of partial differential equation used to describe the dynamic process of coupling diffusion and chemical reaction of matter or information in space [10]. The algorithm itself is constantly being improved and applied in various fields. Liu et al. proposed an efficient quantum algorithm for nonlinear RDE, introducing Carleman linearization method and Allen Cahn equation to extract derivative information by post-processing quantum states. The algorithm was found to achieve faster convergence speed [11]. Xue et al. constructed an RDE with non local spatial memory to simulate the cognitive movement of a single species and studied its dynamics. This study explored the combined effects of perceptual scale and memory delay on system stability and spatiotemporal dynamics through Turing Hopf bifurcation and double Hopf bifurcation. The perceptual scale and memory delay could be analyzed through dynamics [12]. Zayed et al. studied solitary wave solutions in stochastic RDEs and revealed new triangular and hyperbolic stochastic exact solutions by introducing two different integration methods and concatenating them. In numerical simulations, the newly discovered solutions using this method were effective at the application level [13]. Agresti A studied the noise regularization problem of RDE groups with quality control. Experimental results showed that moderate transmission type random multiplicative perturbations had regularization effects [14]. Hadhoud et al. proposed a shift configuration scheme for solving 2D fractional order coupled RDE. This method determined the expansion coefficients by simplifying the boundary conditions into a system of ordinary differential equations with these coefficients, transforming the 2D spatiotemporal fractional order coupled RDE into an algebraic equation system. The proposed method exhibited excellent performance and efficiency [15]. Overall, RDE can be applied in image processing, with strong potential for development in areas such as image denoising, restoration, and segmentation [16]. Barbu T proposed a new framework for the problem of automatic vehicle detection and tracking. This framework combined DL with target detection technology based on Gaussian mixture models to detect moving vehicles and determine the correspondence between video targets between consecutive frames through multi-scale analysis. [17]. Hagemann et al. proposed an infinite-dimensional diffusion model for the finite-dimensional Stochastic Banach Space Diffusion Models (SBDMs) in image generation, which models the training data over rectangular regions. This model achieved higher-resolution image generation and improved training efficiency. The results showed that this method could effectively overcome the shortcomings of existing methods and show practical advantages on synthetic Gaussian mixture samples, MNIST datasets, and datasets generated by nonlinear 2D reaction-diffusion equations. [18]. The specific comparison of the above-mentioned literature is shown in Table 1.

Table 1: Literature review table

Literature	Method	Advantages	Limitations
Literature [5]	Post-processing method for magnetic resonance images based on DL	It has a remarkable effect on improving image quality and correcting artifacts	The model decision-making mechanism is like a "black box", and its application in security-sensitive fields is limited
Literature [6-7]	An underwater image enhancement method based on the fusion of multi-interval sub-histogram perspective equalization and weighted wavelet visual perception	It is significantly superior to the existing methods in both qualitative and quantitative aspects	For specific degradation models (such as underwater), the generalization ability remains to be verified
Literature [8]	A low-light image enhancement method based on the diffusion model introduces a high-frequency recovery module	Better fine recovery has been achieved and efficiency has been significantly improved	Diffusion models generally have the problems of long processing time and high consumption of computing resources
Literature [9]	Agricultural product disease identification based on CNN	It outperforms other existing methods in terms of defect classification accuracy	Strong reliance on large-scale labeled data for training leads to high deployment costs
Literature [10]	Reaction-diffusion equation with non-local spatial memory	It can simulate cognitive movements and reveal the combined influence of perceptual scale and memory delay on system dynamics	It focuses on theoretical dynamic analysis, but the specific application paradigm in image processing is not clear
Literature [11]	The solitary wave solution of the random reaction-diffusion equation	A new stochastic exact solution was revealed, and its	The construction of solutions strongly depends on the form of

	is solved by the series integration method	application effect in numerical simulation was remarkable	the equation, and universal methods are still under exploration
Literature [12]	Study the noise regularization of reaction-diffusion equations with quality control	Experiments show that random multiplicative perturbations have a regularization effect	Theoretical research is rather abstract, and the connection with specific image processing tasks needs to be further established
Literature [16]	A shift configuration scheme for solving 2D fractional-order coupled reaction-diffusion equations	It demonstrated excellent computing performance and efficiency	The method is specifically designed for fractional calculus scenarios and does not have a direct advantage in integer-order problems
Literature [17]	An automatic vehicle detection and tracking framework combining DL with object detection technology based on Gaussian mixture model	The detection of moving vehicles was achieved, and the inter-frame target correspondence was determined through multi-scale analysis	For systems engineering, the theoretical basis and interpretability of the underlying processing units have not been deeply explored
Literature [18]	An infinite-dimensional SBDM for image generation	It can achieve higher-resolution image generation and improve training efficiency	The model is complex, and the performance improvement comes at the cost of high computational complexity

To sum up, current IPT research, especially DL methods, still faces some inherent limitations while achieving performance improvements. Firstly, there is poor physical interpretability. DL models are like "black boxes" whose decision-making mechanisms are difficult to understand, limiting their application in security-sensitive fields. Secondly, there is a strong dependence on data and computing power. High performance heavily depends on large-scale labeled data and powerful computing resources, creating a contradiction between generalization ability and deployment cost. The last issue is that it is difficult to balance computational efficiency and accuracy. Although complex network structures can improve accuracy, they often lead to high computational overhead and a large number of iterations, making it difficult to meet the needs of real-time processing. In addition, traditional reaction-diffusion models have good physical interpretability. However, its application in image processing often relies on empirical parameter adjustment, has limited ability to handle complex textures and noise, and fails to be deeply integrated with modern data processing frameworks. Given this, this study proposes an IPT based on RDE, which combines the FitzHugh-Nagumo (FHN) model with the Cellular Neural Network (Cellular-NN) to construct a new FHN-Cellular-NN image processing model. This model compensates for the shortcomings of traditional algorithms including insufficient computing power, strong data dependence, and poor real-time performance. The innovation of the research lies in the combination of Cellular-NN and FHN, which achieves a balance between efficiency, accuracy, and physical interpretability in image processing through dynamic driven feature optimization. Secondly, using dynamic analysis tools such as Turing instability analysis, waveform analysis, steady-state and stable point value analysis, FHN-Cellular-NN is deconstructed from the perspective of dynamic systems. This study helps to reveal the intrinsic evolution mechanism of the model, optimize parameter design, and enhance the physical interpretability and robustness of the algorithm.

2 Methods and materials

2.1 Construction of image processing model based on RDE

To address the limitations of existing image processing models in terms of computational efficiency, data dependency, and physical interpretability, this study aims to construct a new image edge detection model based on FHN-CNN. The study proposes a core hypothesis: By mapping the dynamic characteristics of the FHN model to the local coupling architecture of CNN and using dynamical system theory tools such as Turing instability for regulation, the constructed model can maintain high edge detection accuracy while reducing computational complexity and the number of iterations. Next, the study will elaborate in detail on the construction process, dynamic analysis, and solution methods. In digital image processing, the choice of color model directly affects the processing effect. The commonly used color models for hardware devices include Red-Green-Blue (RGB), Cyan Magenta Yellow (CMY), and Hue Saturation Value (HSV). Due to the differences in numerical representation between RGB and CMY models and human perception, while HSV models are more in line with human visual characteristics [19], it is often necessary to convert RGB models to HSV models in the image processing process of RDE. The specific processing flow is shown in Figure1. The FHN equation is selected as the core dynamic equation for constructing the proposed model. Its reaction-diffusion form is as follows: Step 1 is to define the core dynamic equation. Step 2 is the integration with Cellular-BN. Step 3 is to

construct the matrix form and boundary conditions. Step 4 is the edge detection task of the image, which can be completed by solving the above coupled ordinary differential equation system.

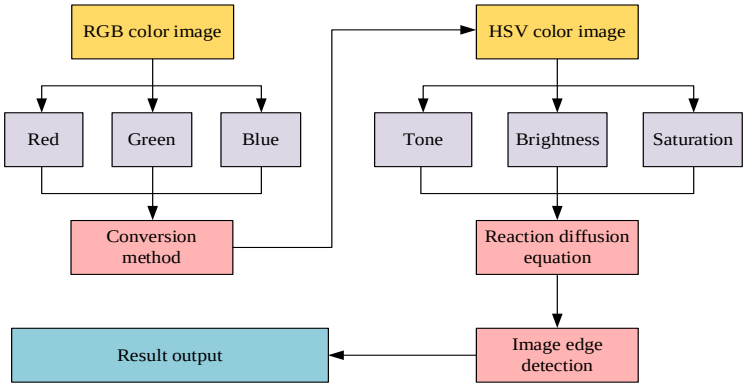

Figure1: Color model conversion

In Figure1, the RGB color image can be decomposed into pixels of the three primary colors of red, green, and blue. The three primary colors correspond to different values in their color model space, and the values of the three primary colors are mapped one-to-one to the HSV color space through conversion methods to obtain HSV color images. The three elements of hue, brightness, and saturation separated from HSV color images are the input values suitable for RDE processing. This study selects the FHN equation, which is the most suitable for image processing among RDE types, as the algorithm basis for image edge detection [20]. FHN-RDE is shown in equation (1).

$$\begin{cases} \theta_t s = f(s,q) + D_s \nabla^2 s \\ \theta_t q = g(s,q) + D_q \nabla^2 q \end{cases} \quad (1)$$

In equation (1), $\theta_t s$ is the time derivative of the membrane potential. $\theta_t q$ is the time derivative of the recovery variable. s is the neuronal membrane potential. q is the recovery variable. D_s and D_q are diffusion coefficients. ∇^2 is the Laplacian operator. The expanded form after substituting equation (1) into the function is shown in equation (2).

$$\begin{cases} \frac{\theta s}{\theta t} = \delta[D_s \nabla^2 s + s(a-s)(s-1) - q] \\ \frac{\theta q}{\theta t} = s - bq + D_q \nabla^2 q \end{cases} \quad (2)$$

In equation (2), $\frac{\theta s}{\theta t}$ is the time derivative of the membrane potential. $\frac{\theta q}{\theta t}$ is the time derivative of the recovery variable. t is time. δ is the external stimulus current. a is the activation threshold parameter. b is the attenuation coefficient of the recovery variable. The unfolded original FHN RDE is obtained through equations (1) and (2). The equation cannot be directly used for image edge detection, so this study introduces a locally interconnected nonlinear simulation dynamic system Cellular-NN to construct an image processing model based on RDE [21]. This study names the new model FHN-Cellular-NN. The Cellular-NN structure is shown in Figure2.

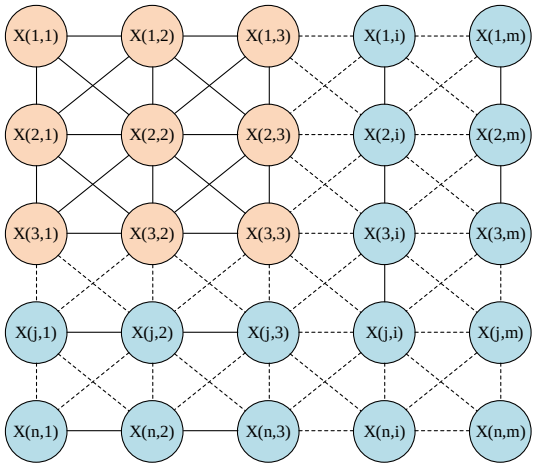

Figure 2: Cellular-NN dynamical system structure

In Figure2, Cellular-NN adopts a grid topology structure, and its core architecture consists of n rows and m columns of regularly arranged units. Each unit $X`_{ji}$ corresponds to the position of the j-th row and i-th column in the array. The connection characteristics of this network are manifested as local coupling, where each unit only establishes electrical connections with its directly adjacent units. This neighborhood interconnection mechanism significantly reduces the complexity of the system. The state function of the Cellular-NN dynamical system is shown in equation (3).

$$X`_{ji} = \sum_{X(k,l)\in V_r(j,i)} \alpha(j,i,k,l) H_1 + \sum_{X(k,l)\in V_r(j,i)} \beta(j,i,k,l) H_2 - X_{ji} \quad (3)$$

In equation (3), $X`_{ji}$, X_{ji}, and $X(k,l)$ are the updated state, current state, and neighboring units of unit

$X(j,i)\cdot V_r(j,i)$ is connected to unit $X(j,i)\cdot$ r is the adjacency radius of the unit. $\alpha(j,i,k,l)$ is the feedback matrix. $\beta(j,i,k,l)$ is the control matrix. H_1 is the output connection weight of $X(k,l)$ and $X(j,i)\cdot$ H_2 is the input connection weight for $X(k,l)$ and $X(j,i)\cdot$ The combination of FHN and Cellular-NN first introduces the Laplacian operator, as shown in equation (4).

$$\begin{aligned}\nabla^2 &= (x,y+1)+(x,y-1)+(x+1,y)\\ &\quad +(x-1,y)-4(x,y)\end{aligned} \tag{4}$$

In equation (4), x is the value on the x axis. y is the numerical value on the y axis. (x,y) represents the coordinate point. Secondly, each (x,y) two-dimensional coordinate point is considered as a unit of the Cellular-NN dynamical system, so substituting equation (4) into equation (2) yields equation (5).

$$\begin{cases} s_{j,i}` = -s_{j,i}+\delta D_s s_{j,i+1}+\delta D_s s_{j,i-1}+\delta D_s s_{j+1,i}+\delta D_s s_{j-1,i}+\\ \quad [1+\delta a-4\delta D_s+\delta(1+a)s_{j,i}-\delta s_{j,i}^2]s_{j,i}-\delta q_{j,i} \\ q_{j,i}` = -q_{j,i}+D_q q_{j,i+1}+D_q q_{j,i-1}+D_q q_{j+1,i}+\\ \quad D_q q_{j-1,i}+(1-4D_q-b)q_{j,i}+s_{j,i}\end{cases} \tag{5}$$

In equation (5), $s_{j,i}`$, $q_{j,i}`$, $s_{j,i}$, and $q_{j,i}$ represent the membrane potential time derivative, recovery variable time derivative, membrane potential, and recovery variable of the j-th row and i-th column units. If $X`_{ji}$ in equation (3) can be regarded as $s_{j,i}`$ in equation (5), then the matrix of FHN-Cellular-NN membrane potential dimension is shown in equation (6).

$$\begin{cases} \alpha_{s,s}=\begin{bmatrix} 0 & \delta D_s & 0 \\ D_s & 1+\delta a-4\delta D_s+\delta(1+a)x-\delta x^2 & \delta D_s \\ 0 & \delta D_s & 0 \end{bmatrix} \\ \alpha_{q,s}=\begin{bmatrix} 0 & 0 & 0 \\ 0 & -\delta & 0 \\ 0 & 0 & 0 \end{bmatrix} \\ \beta_{s,s}=\begin{bmatrix} 0 & 0 & 0 \\ 0 & 0 & 0 \\ 0 & 0 & 0 \end{bmatrix} \end{cases} \tag{6}$$

In equation (6), $\alpha_{s,s}$ and $\beta_{s,s}$ are the coupling feedback matrix and coupling control matrix between membrane potential and membrane potential. $\alpha_{q,s}$ is the coupling feedback matrix of membrane potential and recovery variable. If $X`_{ji}$ in equation (3) can be regarded as $q_{j,i}`$ in equation (5), then the FHN-Cellular-NN restores the matrix of variable dimensions as shown in equation (7).

$$\begin{cases} \alpha_{q,q}=\begin{bmatrix} 0 & D_q & 0 \\ D_q & 1-4D_q-b & D_q \\ 0 & D_q & 0 \end{bmatrix} \\ \alpha_{q,s}=\begin{bmatrix} 0 & 0 & 0 \\ 0 & 1 & 0 \\ 0 & 0 & 0 \end{bmatrix} \\ \beta_{q,q}=\begin{bmatrix} 0 & 0 & 0 \\ 0 & 0 & 0 \\ 0 & 0 & 0 \end{bmatrix} \end{cases} \tag{7}$$

In equation (7), $\alpha_{q,q}$ and $\beta_{q,q}$ are the coupling feedback matrix and coupling control matrix between two recovery variables. To eliminate the arbitrariness of FHN-Cellular-NN solutions and ensure the uniqueness of numerical solutions, this study constructs discrete boundary condition equations. The discrete boundary condition equation based on rows is shown in equation (8).

$$\begin{cases} R_{j,-1}=R_{j,0} \\ R_{j,m-1}=R_{j,m} \end{cases},\ j=0,1,...,n-1 \tag{8}$$

In equation (8), $R_{j,-1}$ and $R_{j,0}$ are the values of row j, column -1, and row j, column 0 of the matrix. $R_{j,m-1}$ and $R_{j,m}$ are the values of the j-th row, $m-1$-th column, and j-th row, m-th column of the matrix. The column based discrete boundary condition equation is shown in equation (9).

$$\begin{cases} R_{-1,i}=R_{0,i} \\ R_{n-1,i}=R_{n,i} \end{cases},i=0,1,...,m-1 \tag{9}$$

In equation (9), $R_{-1,i}$ and $R_{0,i}$ represent the values of row -1, column i, and row i of the matrix. $R_{n-1,i}$ and $R_{n,i}$ are the values of row $n-1$, column i, and row n, column i of the matrix. The final solution of FHN-Cellular-NN can be obtained by combining equations (8), (9), and (5). The discrete boundary condition adopted here mathematically corresponds to the Neumann boundary condition (zero flow condition). The physical meaning of this condition is to assume that the pixel values outside the image boundary are the same as those at the very edge, thereby numerically eliminating the false gradient at the boundary. In summary, the functional expression of FHN-Cellular-NN is obtained through equations (1) to (5), and the solution method of FHN-Cellular-NN is obtained through equations (6) to (9).

After completing the mathematical construction and discretization solution of the FHN-Cellular-NN model, a core question emerges: Does this model have the ability to generate stable and controllable patterns during the dynamic evolution process to reliably perform the image edge detection task? To solve the above problems and deeply understand the intrinsic behavior and stability of the model, the study has shifted from the perspective of

dynamical system theory to conduct an in-depth dynamic analysis of FHN-Cellular-NN. This analysis aims to provide a theoretical basis for the selection of model parameters by exploring the Turing instability, steady-state characteristics, and gradient evolution laws, and to clarify the dynamic basis for achieving spontaneous edge emergence in image processing. The study adopts the finite difference method to discretize the reaction-diffusion equation. Specifically, the spatial derivative is discretized using the second-order central difference scheme. The temporal derivative is advanced using the explicit Euler method. The choice of this explicit format is based on its simple implementation and high compatibility with the local coupling characteristics of Cellular-NNs, facilitating parallel computing on grid cells.

2.2 Dynamic analysis of image processing model based on RDE

The image processing model from a dynamic perspective actually views image processing tasks as a dynamic evolutionary process. Conducting dynamic analysis on FHN-Cellular-NN can help clarify the interaction mechanism between diffusion and reaction, and provide criteria for establishing the dynamic stability of non-equilibrium systems. This study explores the universality of non-equilibrium systems by analyzing the Turing instability of FHN-Cellular-NN [22]. The main idea is to establish a quantitative criterion for diffusion driven instability through linear stability analysis and characteristic equation solving. The characteristic equation of equation (2) at point $(0,0)$ is shown in equation (10).

$$\Omega^2+\left[a\delta+b+(D_s+D_q)\frac{c^2}{d^2}\right]\Omega +\left(a\delta+D_s\frac{c^2}{d^2}\right)\left(b+D_q\frac{c^2}{d^2}\right)+\delta=0 \tag{10}$$

In equation (10), Ω is a constant. c and d are random variables. Assuming $c=0$, equation (10) is transformed into equation (11).

$$\Omega^2+(a\delta+b)\Omega+(ab+1)\delta=0 \tag{11}$$

In equation (11), Ω is a constant. a is the activation threshold parameter. b is the attenuation coefficient of the recovery variable. δ is the external stimulus current. When $\begin{cases}a\delta+b>0\\ab+1>0\end{cases}$, equation (11) has a root with a negative real part, and when $\begin{cases}a\delta+b>0\\ \delta=-\dfrac{b}{a}\end{cases}$, bifurcation occurs. When $c\neq 0$, equation (10) can be written as equation (12).

$$\begin{cases}\Omega^2+F_c(\delta)\Omega+D_c(\delta)=0\\ F_c(\delta)=a\delta+b+(D_s+D_q)\dfrac{c^2}{d^2}>0\\ D_c(\delta)=D_sD_q\dfrac{c^4}{d^4}+(a\delta D_q+bD_s)\dfrac{c^2}{d^2}+(ab+1)\delta=0\end{cases} \tag{12}$$

In equation (12), $F_c(\delta)$ and $D_c(\delta)$ are newly constructed functions. By analyzing the solutions of characteristic equation (10) under different parameter ranges, the parameter values for the Turing instability of FHN-Cellular-NN are determined. The determined values of the parameter group are substituted into equation (10) for solving, resulting in the waveform diagram when instability occurs, as shown in Figure3.

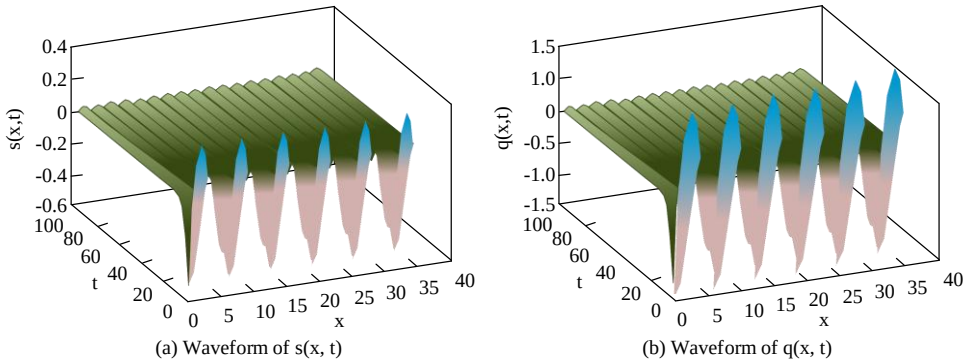

(a) Waveform of s(x, t) (b) Waveform of q(x, t)

Figure 3: FHN-Cellular-NN waveform diagram

Figure3 shows the waveform of membrane potential dimension $s(x,t)$ and recovery variable dimension $q(x,t)$ for $a=2$, $D_s=6$, $D_q=0.001$, and $b=-0.1$. When the above parameters are used, the FHN-Cellular-NN exhibits Turing instability, and the steady state $(0,0)$ is unstable, resulting in a new non-steady state solution. Based on the dynamic analysis of the Turing instability of FHN-Cellular-NN, this study obtains the parameter solution of the FHN-Cellular-NN

model in a stable state. Next, further analysis is conducted on the mono-stable and multi-steady states of FHN-Cellular-NN under different a and b values, as shown in Figure4.

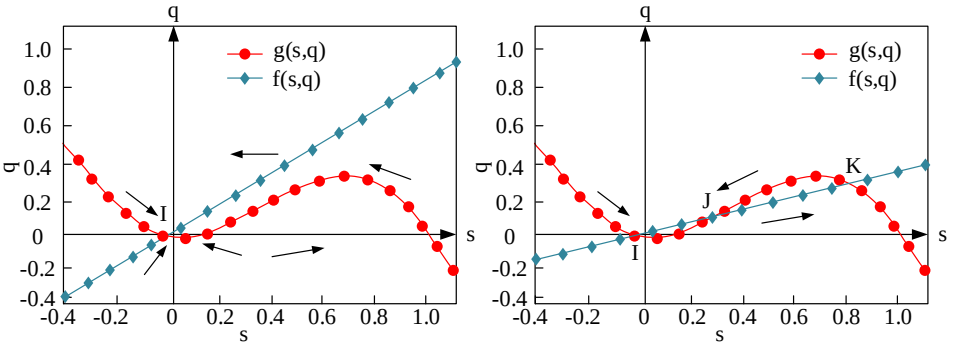

Figure 4: Analysis of FHN-Cellular-NN single and multi-steady states

Figure4 shows the analysis of the results obtained by adjusting the values of a and b to find the monostable and bistable parameter solutions for FHN-Cellular-NN. In Figure4 (a), the g(s,q) and f(s,q) functions of FHN-Cellular-NN have a stable point I, and values greater than this stable point are considered edge points. In Figure4 (b), the function has three stable points I, J, and K. That is, at these values of a and b, FHN-Cellular-NN is a multi-stable system with multiple stable points. The smaller the stable point value, the more complete the detection coverage of image edges, but the processed image noise will increase. On the contrary, the smaller the detection coverage of image edges, the finer the edge processing and the lower the noise [23]. Usually, multiple experiments are required to find a moderate value for the stable point. The mono-stable state is relatively easier to adjust because it only has one stable point. Therefore, this study selects a mono-stable system and adjusts the stable point of FHN-Cellular-NN to find its suitable value. Firstly, the stable point value is defined as ∂, and the diffusion equation of ∂ can be expressed as equation (13).

$$\partial(x) = Q(s_0(x); U, G) \tag{13}$$

In equation (13), $\partial(x)$ is the diffusion equation of ∂. U is the diffusion coefficient. G and Q are constants. $s_0(x)$ is the diffusion function for restoring the variable dimension. Equation (13) can be directly used for detecting image edges, but it still has some shortcomings. When the diffusion coefficient increases, the distance between edges will increase, resulting in blurred edges of the image. Therefore, this study further optimizes the diffusion coefficient U to avoid detecting edge blurring. The functional expression for constructing the diffusion coefficient U is shown in equation (14).

$$U = u(\varepsilon) = \frac{1}{1+(\varepsilon / k)^2} \tag{14}$$

In equation (14), $u(\varepsilon)$ is a function expression of the adjustment coefficient. ε is the normalized value of each pixel in the image. k is a constant. The acquisition of ε can be expressed as equation (15).

$$\varepsilon = |\ \nabla \mathrm{s}\ | = \sqrt{B_x^2 + B_y^2} \tag{15}$$

In equation (15), ε is the normalized value of each pixel in the image. $\nabla \mathrm{s}$ is an operator for restoring variable dimensions. B_x and B_y are specific matrices. The specific matrix of B_x and B_y is given by equation (16).

$$\begin{cases} B_x = \begin{pmatrix} -1 & 0 & 1 \\ -2 & 0 & 2 \\ -1 & 0 & 1 \end{pmatrix} \sigma_0 \\ B_y = \begin{pmatrix} -1 & -2 & -1 \\ 0 & 0 & 0 \\ 1 & 2 & 1 \end{pmatrix} \sigma_0 \end{cases} \tag{16}$$

In equation (16), σ_0 is the original input image. Equations (13) to (16) introduce a method of adjusting the stable point value of FHN-Cellular-NN to a moderate value, enabling FHN-Cellular-NN to have adaptive control capability for stable point values. In the process of feature extraction from digital images, region boundaries often exhibit significant gradient changes. At this point, the adjustment function will automatically converge to the minimum value in the high gradient region, achieving automatic termination of boundary positioning and ensuring accurate convergence of the contour line to the target edge position. The gradient variation of the reaction-diffusion system is shown in Figure5.

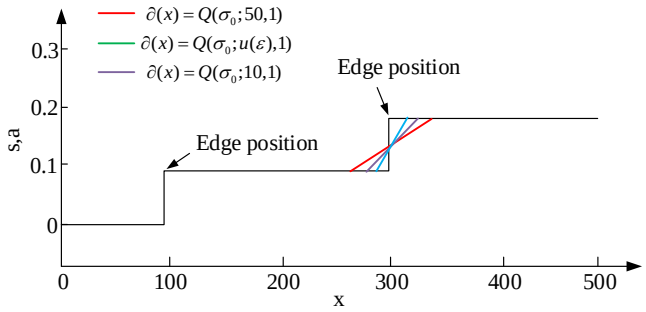

Figure 5: Gradient variation of reaction-diffusion system

Figure5 shows the gradient changes of diffusion distribution curves $\partial(x)=Q(\sigma_0;50,1)$, $\partial(x)=Q(\sigma_0;10,1)$, and $\partial(x)=Q(\sigma_0;u(\varepsilon),1)$ at parameter values $b=2$, $\varepsilon=10^3$, $D_S=0.5$, and $D_q=4$. When the stable point value used is not appropriate, the diffusion distribution curve will vibrate in two directions, producing double edges and blurring the image edges. After introducing the adjustment function, the $\partial(x)=Q(\sigma_0;u(\varepsilon),1)$ diffusion distribution curve can be accurately located at the edge of the image. This study conducts a dynamic analysis of an image processing model based on RDE, and determines the parameter values for the Turing instability of FHN-Cellular-NN by solving the characteristic equation. Based on the found parameter values, the waveform, steady-state, and stable point values of FHN-Cellular-NN are analyzed. Finally, a method is introduced to adjust the stable point value of FHN-Cellular-NN to a moderate value. Based on the above two sections, an IPT framework based on RDE is constructed from the perspective of dynamical systems. The pseudo-code of the FHN-Cellular-NN method is shown in Table 2.

Table 2: FHN-Cellular-NN pseudo-code

```
// Pseudo-code for RDE-based Image Processing Model (FHN-Cellular-NN)
function Main(image_path):
    image = LoadImage(image_path)
    hsv_image = RGBToHSV(image) // Convert RGB to HSV
    hue, saturation, brightness = ExtractHSVComponents(hsv_image)

    // FHN-RDE Computation
    membrane_potential, recovery_variable = ComputeFHN_RDE(hue, saturation, brightness)

    // Initialize and update Cellular-NN
    Cellular-NN_structure = InitializeCellular-NN()
    UpdateCellStates(Cellular-NN_structure, membrane_potential, recovery_variable)

    // Perform dynamic analysis for edge detection
    waveform = DynamicAnalysis(Cellular-NN_structure)

    // Evaluate performance
    metrics = EvaluatePerformance(waveform)
    Print("EPI: ", metrics.EPI, ", PFOM: ", metrics.PFOM)

// FHN-RDE Computation
function ComputeFHN_RDE(hue, saturation, brightness):
    for each time_step:
        for each pixel:
            UpdateMembranePotential(pixel)
            UpdateRecoveryVariable(pixel)
    return membrane_potential, recovery_variable

// Initialize Cellular-NN
function InitializeCellular-NN():
    CreateGrid(n_rows, m_columns)
    ConnectCells()
```

```
    return Cellular-NN_structure

// Update Cellular-NN cell states
function UpdateCellStates (Cellular-NN_structure, membrane_potential, recovery_variable):
    for each cell in Cellular-NN_structure:
        neighbors = GetNeighbors(cell)
        updated_state = ComputeNewState (cell, neighbors, membrane_potential, recovery_variable)
        SetCellState(cell, updated_state

// Dynamic Analysis of the model
function DynamicAnalysis (Cellular-NN_structure):
    parameters = AnalyzeParameters (Cellular-NN_structure)
    return ComputeWaveform (parameters)

// Run the main function
Main(image_path)
```

3 Results

3.1 IPT performance testing based on RDE

After completing the theoretical construction and dynamic characteristic analysis of the FHN-Cellular-NN model, the study quantitatively evaluates its actual performance through a series of systematic experiments. The following section first presents the performance test results of this model on the standard image library, comparing it with the classical algorithm to verify its advantages in edge detection accuracy and computational efficiency. Subsequently, through numerical simulation, the convergence behavior of the model and the generation mechanism of the Turing mode are deeply revealed from the perspective of the dynamical system. Finally, through parameter sensitivity analysis, the identification and verification of the optimal model configuration are completed.

In the tested hardware environment, the CPU is Intel Core i9-13900K, the GPU is NVIDIA RTX 4090, and the memory is 64GB DDR5. The software development tool is Ubuntu 22.04 LTS system. The experimental dataset randomly selects 500 images covering natural scenes, objects, and people from the validation set of the MS COCO 2017 dataset. All input images are uniformly scaled to a resolution of 512×512 pixels. The pixel values are normalized from the integer range of 0-255 to the floating-point range of 0-1 for model processing. Baseline methods used for comparison include Sobel, Roberts, Canny and traditional CNN edge detection methods. All methods are implemented according to the standards of the OpenCV and Scikit-image libraries and uniformly use the best default parameters determined by grid search. In terms of evaluation criteria, the edge preservation index is used to quantify the similarity between the processed image and the original image in non-edge areas. The closer its value is to 1, the stronger the edge preservation ability. The Pratt quality factor comprehensively evaluates the edge detection accuracy by calculating the matching degree of position and integrity between the detected edge and the real edge, with its maximum value being 1. To verify the effectiveness of FHN-Cellular-NN, this study conducts performance tests on classic image edge detection algorithms such as Sobel, Roberts, Canny, and Cellular-NN, and compares the test results with FHN-Cellular-NN. The test mainly refers to two indicators, Pratt's Figure of Merit (PFOM), and Edge Position Inaccuracy (EPI), as shown in Figure6.

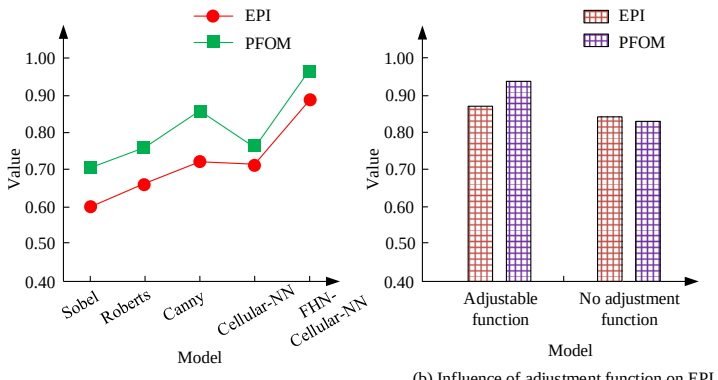

(a) EPI and pfom test results of different models

(b) Influence of adjustment function on EPI and pfom test results

Figure 6: EPI and PFOM test results

In Figure6 (a), the EPI of FHN-Cellular-NN is 0.89 and the PFOM is 0.95. Comparison shows that FHN-Cellular-NN has significantly higher indicators than other algorithms. In Figure6 (b), the EPI and PFOM with adjustment function are 0.87 and 0.94, while the EPI and PFOM without adjustment function are 0.83 and 0.81. However, the two indicators with adjustment function are higher. FHN-Cellular-NN introduces a tuning function, which outperforms the comparison model in terms of performance. To test the computational efficiency of FHN-Cellular-NN, further comparative experiments are conducted. By comparing the time cost and iteration times of different algorithms to complete a detection, the computational efficiency of different algorithms is quantitatively analyzed, as shown in Figure7.

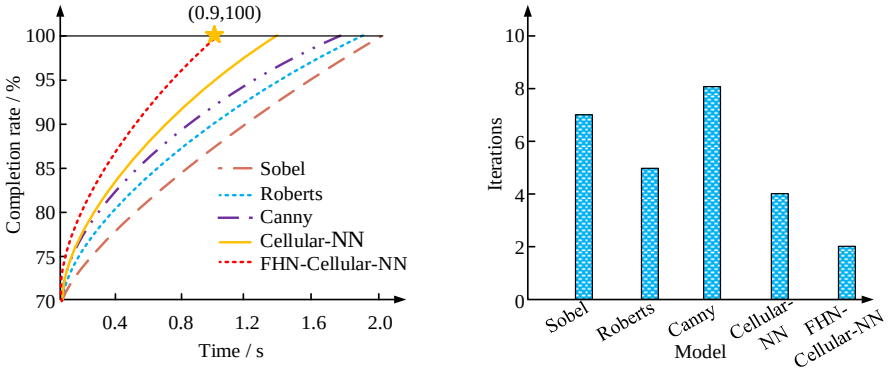

(a) Time cost results of different models (b) Iteration results of different models

Figure 7: Results of time cost and iteration times for different models

In Figure7 (a), the time overhead for Sobel, Roberts, Canny, Cellular-NN, and FHN-Cellular-NN to complete one detection is 2 s, 1.9 s, 1.7 s, 1.4 s, and 0.9 s, with FHN-Cellular-NN having the lowest time overhead. Compared to other algorithms, FHN-Cellular-NN has significantly improved computational efficiency. In Figure7 (b), the iteration times of the five algorithms in one detection are 7, 5, 8, 4, and 2. When FHN-Cellular-NN performs computational tasks, it has fewer iterations compared to the comparison model, which better meets the real-time requirements of the algorithm. To further verify the computational efficiency of FHN-CNN from the underlying mechanism, the time complexity and space complexity of each algorithm are compared and analyzed. The results are shown in Table 3. Time complexity reflects the trend of an algorithm's execution time growing with the input scale, while space complexity reflects the algorithm's consumption of memory resources.

Table 3: Comparison of the complexity of different edge detection algorithms

Algorithm	Sobel	Roberts	Canny	CNN	FHN-CNN
Time complexity	O(n)	O(n)	O(n log n)	O(n)	O(n)
Space complexity	O(n)	O(n)	O(n)	O(n)	O(n)
Average number of iterations	49	38	56	28	14
Average single test time (s)	2	1.9	1.7	1.4	0.9

In Table 3, although Sobel, Roberts, and CNN have a linear time complexity of O(n), their number of iterations and actual running time are both higher than those of FHN-CNN. The Canny algorithm has a time complexity of O(n log n) because it includes steps such as non-maximum suppression and double-threshold connection, and its efficiency disadvantage is more obvious when dealing with large-scale images. The FHN-CNN model maintains the linear complexity, and its core advantage lies in transforming the static task of edge detection into a rapidly converging dynamic process through the dynamic characteristics of the reaction-diffusion system. In Table 3, the average number of iterations of FHN-CNN is only 14, which is significantly lower than that of other comparison models. This is attributed to the analysis of Turing instability and the adaptive control of stability points during the model's construction, enabling the system to rapidly evolve from the initial state to the target edge state. As a result, while maintaining a low computational complexity, the actual running time has been significantly reduced.

3.2 Numerical simulation based on RDE from the perspective of dynamical system

Through performance testing of FHN-Cellular-NN algorithm, it has been preliminarily confirmed that FHN-Cellular-NN has slightly improved algorithm performance compared to traditional algorithms. This study further conducts numerical simulations on FHN-Cellular-NN to analyze the long-term behavior of

the algorithm from the perspective of dynamical systems. There are two types of experiments set up for numerical simulation. One is the convergence order test of the algorithm extrapolated solutions in both spatial and temporal directions, and the other is the Turing spot generation experiment. This study sets up a numerical example to verify the convergence of discrete schemes in space and time, as shown in Figure8.

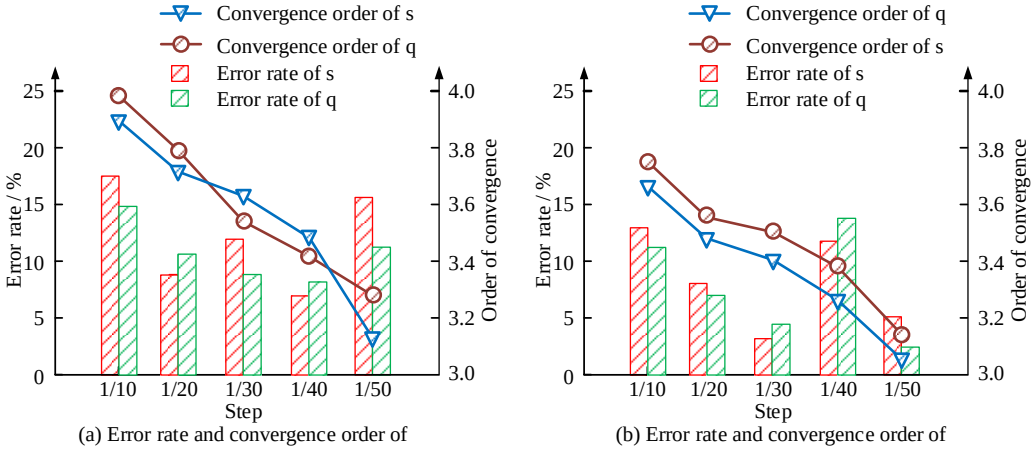

Figure 8: Error rate and convergence order of extrapolation solution in spatiotemporal direction

In Figure8 (a), the convergence order of vectors s and q in RDE shows a monotonically decreasing trend as the spatial step size decreases. In the solution of dynamical systems, monotonically decreasing convergence order means that stability is maintained throughout the entire convergence process. The error rate of vectors s and q remains below 20% and has no obvious pattern, which is a normal phenomenon. In Figure8 (b), the convergence order of vectors s and q in RDE monotonically decreases with decreasing time step. The test results in the time direction are roughly consistent with those in the spatial direction. The discrete format can achieve a very good convergence accuracy and reach the optimal convergence order. Turing pattern generation is a mathematical theoretical model that describes the spontaneous formation of periodic patterns in nature. This study optimizes the parameter configuration of the reaction-diffusion model by conducting a Turing spot generation experiment on FHN-Cellular-NN. The spatial step size is 1/50, the time step size is 1/10, and the vector s is composed of four central points in the initial state. When the parameter a in the vector s changes and b remains unchanged, the evolution process is shown in Figure9.

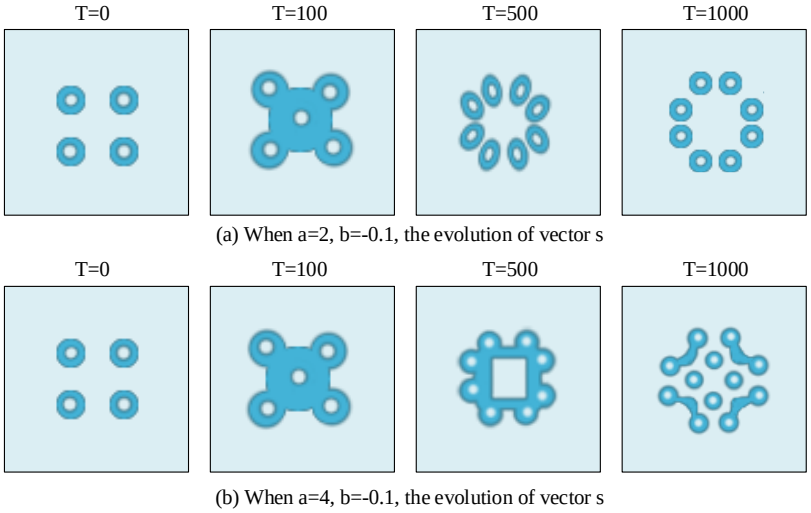

Figure 9: Evolution process of Turing spot generation by changing parameter a

In Figure9 (a), the graph shows the Turing spot evolution of vector s over time when a=2 and b=-0.1. The initial four spots gradually elongate and fuse together over time, then split into eight spots, and after migration, the eight spots are finally fixed. In Figure9 (b), the graph shows the Turing spot evolution of vector s over time when a=4 and b=-0.1. Compared with Figure9 (a), the initial four spots in the early stage still follow the step of first elongating and then fusing. In the later stage, the spots are not completely separated, forming strip-shaped spots,

and then migrating to form a new shape combining strip-shaped spots with individual spots. When the parameter a in vector s remains unchanged and b changes, the evolution process is shown in Figure10.

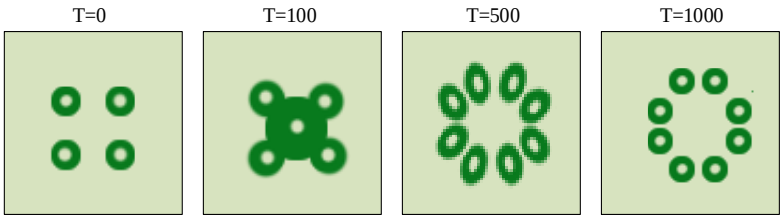

(a) When a=2, b=-0.1, the evolution of vector s

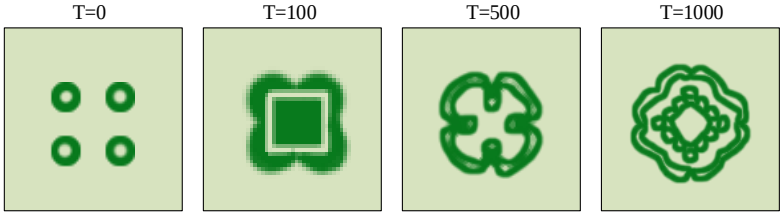

(b) When a=2, b=-0.3, the evolution of vector s

Figure 10: Evolution process of Turing spot generation by changing parameter b

When a=2 and b=-0.1 in Figure10 (a), the evolution process is similar because the parameters are consistent with Figure9 (a). Figure10 (b) shows the Turing pattern evolution of vector s over time when a=2 and b=-0.3. Compared with Figure10 (a), the initial four spots form a new pattern after a brief migration, and then the spots are continuously elongated, eventually merging into a new pattern in the shape of a strip. This study reveals the spontaneous formation mechanism of RDE in image edge detection from the perspective of dynamical systems by setting up Turing spot generation experiments. Turing spot generation relies on the concentration gradient of substances to generate patterns, while image detection relies on pixel gradient detection structures, both of which have the same formation mechanism. The spontaneous pattern formation mechanism demonstrated by the Turing point generation experiment is mathematically isomorphic to the edge detection task. In the Turing system, the patterns originate from the concentration differences caused by diffusion instability in the initial uniform state. In an image, the edges are precisely the gradient regions where the intensity of pixels changes dramatically. Therefore, by regulating the model parameters to guide the Turing pattern to form and stabilize at the image gradient, this mechanism is directly transformed into the precise recognition and enhancement of the image edge. Its spontaneous formation characteristic is the fundamental reason for achieving efficient and low-iteration edge detection. To comprehensively evaluate the performance of the FHN-CNN model, this study quantitatively compares it with the current advanced image processing models based on DL. The comparison models include U-Net, DeepLabv3+, and Holistically-Nested Edge Detection (HED). The experiment is conducted on the publicly available BSDS500 dataset, which contains 500 natural images and their artificially labeled edge truth values. The study adopts the widely used fixed-scale optimal F-score (ODS F-score), single-image optimal F-score (OIS F-score), and Average Precision (AP) as evaluation indicators. The comparison results are shown in Table 4.

Table 4: Performance comparison between FHN-CNN and advanced DL models

Model	U-Net [24]	DeepLabv3+ [25]	HED [26]	FHN-CNN
ODS F-score	0.795	0.812	0.782	0.789
OIS F-score	0.815	0.83	0.804	0.808
AP	0.851	0.865	0.833	0.822
Parameter Quantity (M)	31	59.5	14.7	0.015
Inference Time (ms)	68	112	45	12

According to the performance comparison results shown in Table 4, the FHN-CNN model demonstrates certain comprehensive advantages in the edge detection task. In terms of core performance indicators, the ODS F-score and OIS F-score of FHN-CNN are both higher than those of the HED model and are extremely close to the powerful U-Net model. Meanwhile, its AP value has also reached a level comparable to these advanced DL models, which fully demonstrates its strong competitiveness in detection accuracy. However, the most prominent advantage of FHN-CNN lies in its extremely high computational efficiency. The parameter count of this model is extremely low, only 0.015 million, less than one-thousandth of HED, and far lower than that of large

models such as U-Net and DeepLabv3+. Its single-image reasoning time has also been significantly reduced to as fast as 12 ms, outperforming all comparison models. These data strongly demonstrate that FHN-CNN can achieve edge detection accuracy comparable to advanced DL methods while reducing model complexity and computational overhead by orders of magnitude. This result provides a highly valuable solution for deploying efficient image processing algorithms in resource-constrained environments.

3.3 Parameter tuning of the IPT model based on RDE

The study is conducted to determine the optimal parameter configuration of the FHN-CNN model in image processing tasks through hyperparameter tuning. This process involves a systematic grid search of the key parameters in the response items to evaluate the impact of different parameter combinations on the visual effect and quantitative indicators of edge detection. The experimental results are shown in Figure11.

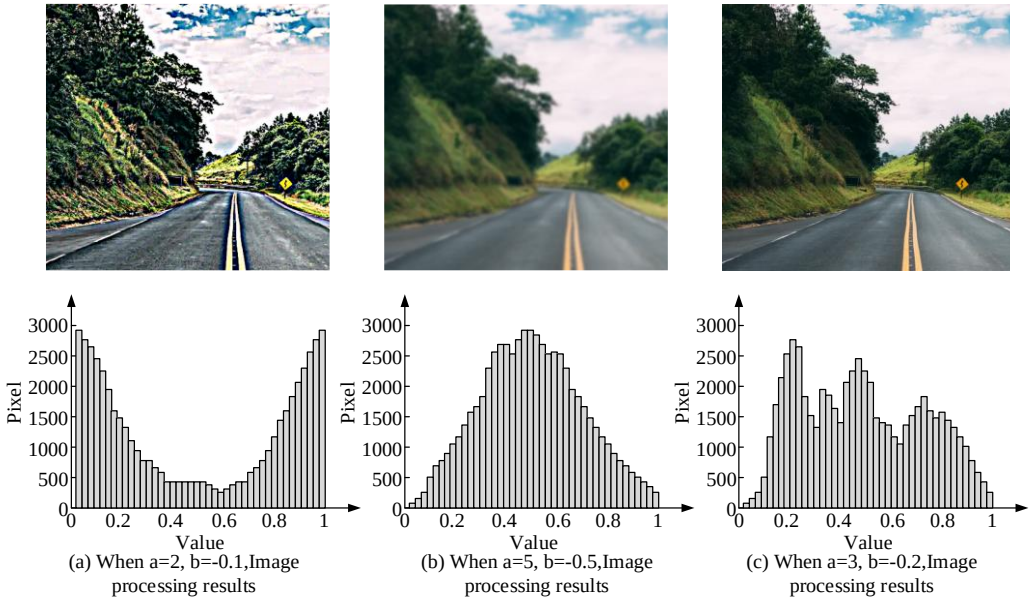

Figure 11: Image processing results under different parameter groups

In Figure11 (a), when a=2 and b=-0.1, the image undergoes excessive sharpening after edge detection processing. There are a large number of pixel values in the dark area on the left and the bright area on the right, and the histogram trend shows an abnormal state. In Figure11 (b), when a=5 and b=-0.5, the overall effect of the image appears blurry, with significantly too many gray values in the middle of the histogram, making the overall image appear grayish. In Figure11 (c), when a=3 and b=-0.2, the image processing effect is the best, with no obvious overexposure or underexposure, and the overall color of the picture is relatively harmonious. The pixels are concentrated in the middle gray value area and show a fluctuating trend up and down. By comparison, when a=3 and b=-0.2, the algorithm performs the best in image processing tasks. To verify whether RDE and the introduced adjustment function work in FHN-Cellular-NN, this study conducts two image processing experiments based on Figure11 (c) by removing the FHN module and adjustment function from the model, as shown in Figure12.

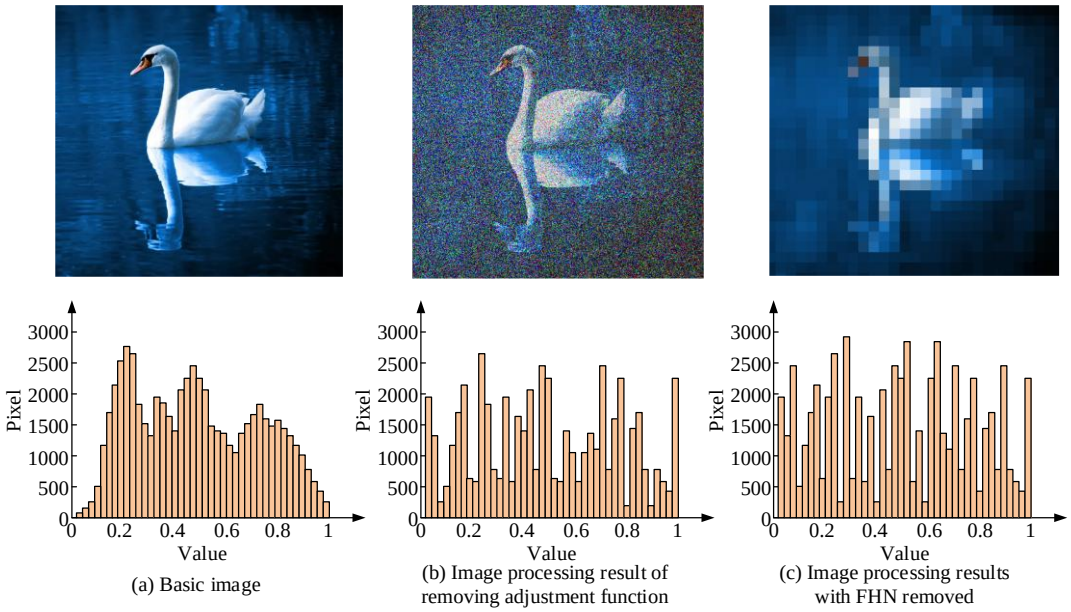

Figure 12: Image processing results after removing algorithm modules

In Figure12 (a), this image serves as the baseline for comparison with other images. In Figure12 (b), after removing the adjustment function, the image generates a lot of noise after processing, and the image quality becomes worse compared to before processing. The values of each part of the histogram are uneven, reflecting poor image processing results. In Figure12 (c), after removing the FHN module, the image generates many mosaics after processing, and the histogram shows an irregular state. The above comparison shows that the histogram trend of the base image is smoother and the image processing effect is better. Therefore, FHN and the introduced adjustment function play an important role in the algorithm, improving its image processing capability.

The FHN-Cellular-NN model has demonstrated potential in multiple practical application scenarios. For instance, in medical image analysis, this model can be used to precisely detect tissue boundaries or lesion areas. In the field of autonomous driving, its efficient edge detection capability helps to identify the contours of roads and obstacles in real time. In remote sensing image processing, the adaptability to complex environments can enhance the accuracy of ground object classification and change detection. These application prospects further highlight the practical value of FHN-Cellular-NN in promoting IPT towards high efficiency and intelligence.

4 Conclusion

For the dynamical systems, the study successfully constructed and verified the FHN-CNN image processing model based on the reaction-diffusion equation. Compared with the existing technologies, this model demonstrated unique advantages, and its outstanding performance was rooted in its inherent dynamic mechanism. The study delved deeply into the intrinsic reasons for performance improvement, clarified the unique value of the power system approach, and reflected on the limitations. The experimental results showed that FHN-CNN outperformed traditional operators and DL models in multiple core indicators of edge detection. Its outstanding performance on EPI (0.89) and PFOM (0.95) demonstrated that the model achieved a good balance between edge positioning accuracy and maintaining structural integrity. More prominently, its extremely low computing time (0.9 seconds) and number of iterations (2 times) highlighted its extraordinary computing efficiency. This performance improvement is not accidental but stems from the dynamic design at the core of the model. Firstly, through Turing instability analysis, a region in the parameter space where a stable pattern can spontaneously form is found. This enables FHN-CNN to achieve efficient edge feature generation without complex multi-layer forward propagation, merely through the dynamic evolution of the system itself. Secondly, the introduced adaptive control mechanism (adjustment function K(s)) plays a key role. This mechanism dynamically adjusts the diffusion behavior based on the local gradient of the image, ensuring that the system can accurately converge to the true edge. It effectively avoids the common edge blurring or double edge phenomena in traditional RDE methods, thereby directly contributing to the improvement of EPI and PFOM indicators. Compared with pure DL models such as U-Net and DeepLabv3+, pure DL models are typical "black boxes", with their decision-making logic deeply hidden in millions or even billions of unexplainable parameters [24]. The construction of FHN-CNN is based on clear physical laws and mathematical equations. Its dynamic behavior, such as the generation of Turing models and the evolution of stability points, can all be strictly mathematically analyzed and intuitively understood through dynamical system theory. The performance of DL models strongly depends on large-scale high-quality

labeled data, and the computational costs of training and inference are high [25]. As a model defined by partial differential equations, the parameters of FHN-CNN have clear physical meanings and do not require data-driven training from scratch.

Although the FHN-CNN model performs well in edge detection tasks, this study still has some limitations. Firstly, in its current form, the model mainly focuses on low-level visual tasks. To directly apply its output to higher-level recognition or segmentation tasks, subsequent processing flows still need to be designed. Future work will explore how to combine FHN-CNN as an interpretable feature extraction front-end with a lightweight decision module to build an end-to-end processing pipeline.

5 Conclusion

In response to the problems of strong noise interference, low edge localization accuracy, multiple iterations, and insufficient adaptability to complex images in existing image processing models, this study proposed an image processing model based on RDE. This model integrated the theoretical tools of dynamical systems into traditional image processing methods by combining FHN and Cellular-NN, thereby achieving efficient application of image processing. The experiment showed that FHN-Cellular-NN had an EPI of 0.89, a PFOM of 0.95, a time cost of 0.9 seconds, and 2 iterations, with significantly better performance than the comparison model. In numerical simulation experiments, the convergence order of RDE vector s and vector q showed a monotonically decreasing trend with the decrease of time step and spatial step, indicating high algorithm stability. Meanwhile, this study also simulated the generation of Turing spots through numerical examples, revealing the spontaneous formation mechanism of RDE in image edge detection from the perspective of dynamical systems. In the model recognition analysis, the optimal parameter set of FHN-Cellular-NN in the direction of image processing was found. In conclusion, through a series of performance tests, numerical simulations, and model recognition, this study has demonstrated the advantages of FHN-CNN in image processing and its ability to meet the requirements of complex image processing. However, the study has the following limitations. Firstly, although it has been compared with DL methods such as U-Net, the comparison scope still needs to be further expanded. Secondly, there is still room for improvement in the diversity and scale of the experimental dataset. Furthermore, the ablation analysis of the respective contributions of CNN and FHN is insufficient. Subsequent research will increase the scale of the dataset, expand the application verification of the model in different types of image processing tasks, and conduct in-depth analysis of the contribution of each module to further enhance the universality and robustness.

References

[1] Kaur N, Jindal N, Singh K. A deep learning framework for copy-move forgery detection in digital images. Multimedia Tools and Applications, 2023, 82(12): 17741-17768. https://doi.org/10.1007/s11042-022-14016-2

[2] Wu Q. Research on deep learning image processing technology of second-order partial differential equations. Neural Computing and Applications, 2023, 35(3): 2183-2195. https://doi.org/10.1007/s00521-022-07017-7

[3] Srinivas N, Mandaloju N, Nadimpalli S V. Leveraging Automation in Software Quality Assurance: Enhancing Defect Detection and Improving Efficiency. International Journal of Acta Informatica, 2024, 3(1): 112-124.

[4] Zangana H M, Mohammed A K, Mustafa F M. Advancements in Edge Detection Techniques for Image Enhancement: A Comprehensive Review. International Journal of Artificial Intelligence & Robotics (IJAIR), 2024, 6(1): 29-39. https://doi.org/10.25139/ijair.v6i1.8217

[5] Chen Z, Pawar K, Ekanayake M, Pain C, Zhong S, Egan G F. Deep learning for image enhancement and correction in magnetic resonance imaging-state-of-the-art and challenges. Journal of Digital Imaging, 2023, 36(1): 204-230. https://doi.org/10.1007/s10278-022-00721-9

[6] Zhou J, Pang L, Zhang D, Zhang W. Underwater image enhancement method via multi-interval subhistogram perspective equalization. IEEE Journal of Oceanic Engineering, 2023, 48(2): 474-488. https://doi.org/10.1109/JOE.2022.3223733

[7] Zhang W, Zhou L, Zhuang P, Li G, Pan X, Zhao W, et al. Underwater image enhancement via weighted wavelet visual perception fusion. IEEE Transactions on Circuits and Systems for Video Technology, 2023, 34(4): 2469-2483. https://doi.org/10.1109/TCSVT.2023.3299314

[8] Jiang H, Luo A, Fan H, Han S, Liu S. Low-light image enhancement with wavelet-based diffusion models. ACM Transactions on Graphics (TOG), 2023, 42(6): 1-14. https://doi.org/10.1145/3618373

[9] Arshaghi A, Ashourian M, Ghabeli L. Potato diseases detection and classification using deep learning methods. Multimedia Tools and Applications, 2023, 82(4): 5725-5742. https://doi.org/10.1007/s11042-022-13390-1

[10] Ninomiya H, Taniguchi M. Traveling Front Solutions of Dimension n Generate Entire Solutions of Dimension $$(n-1) $$ in Reaction-Diffusion Equations as the Speeds Go to Infinity. Archive for Rational Mechanics and Analysis, 2025, 249(1): 1-37. https://doi.org/10.1007/s00205-025-02083-2

[11] Liu J P, An D, Fang D, Wang J, Low G H, Jordan S. Efficient quantum algorithm for nonlinear reaction-diffusion equations and energy estimation. Communications in Mathematical Physics, 2023, 404(2): 963-1020.

https://doi.org/10.1007/s00220-023-04857-9
[12] Xue S, Song Y, Wang H. Spatio-temporal dynamics in a reaction-diffusion equation with nonlocal spatial memory. SIAM Journal on Applied Dynamical Systems, 2024, 23(1): 641-667. https://doi.org/10.1137/22M1543860
[13] Zayed E M, El-Horbaty M, Saad B M, Arnous A H, Yildirim Y. Novel solitary wave solutions for stochastic nonlinear reaction-diffusion equation with multiplicative noise. Nonlinear Dynamics, 2024, 112(22): 20199-20213. https://doi.org/10.1007/s11071-024-10085-0
[14] Agresti A. Delayed blow-up and enhanced diffusion by transport noise for systems of reaction-diffusion equations. Stochastics and Partial Differential Equations: Analysis and Computations, 2024, 12(3): 1907-1981. https://doi.org/10.1007/s40072-023-00319-4
[15] Hadhoud A R, Rageh A A M, Agarwal P. Numerical method for solving two-dimensional of the space and space-time fractional coupled reaction-diffusion equations. Mathematical Methods in the Applied Sciences, 2023, 46(5): 6054-6076. https://doi.org/10.1002/mma.8891
[16] Kaur A, Dong G. A complete review on image denoising techniques for medical images. Neural Processing Letters, 2023, 55(6): 7807-7850. https://doi.org/10.1007/s11063-023-11286-1
[17] Barbu T. Deep learning-based multiple moving vehicle detection and tracking using a nonlinear fourth-order reaction-diffusion based multi-scale video object analysis. Discrete & Continuous Dynamical Systems-Series S, AIMS Journals, 2023, 16(1): 6-32. https://doi.org/10.3934/dcdss.2022083
[18] Hagemann P, Mildenberger S, Ruthotto L, Steidl G, Yang N T. Multilevel diffusion: Infinite dimensional score-based diffusion models for image generation. SIAM Journal on Mathematics of Data Science, 2025, 7(3): 1337-1366. https://doi.org/10.1137/23M1614092
[19] Prakash S R, Singh P N. Background region-based face orientation prediction through HSV skin color model and K-means clustering. International Journal of Information Technology, 2023, 15(3): 1275-1288. https://doi.org/10.1007/s41870-023-01174-1
[20] Kim S, You J. Efficient LUT design methodologies of transformation between RGB and HSV for HSV based image enhancements. Journal of Electrical Engineering & Technology, 2024, 19(7): 4551-4563. https://doi.org/10.1007/s42835-024-01859-y
[21] Chen X, Wang N, Wang K, Chen M, Parastesh F, Xu Q. Coupling dynamics in an FHN bi-neuron model coupled via ReLU function-based locally active memristor. Nonlinear Dynamics, 2024, 112(22): 20365-20379. https://doi.org/10.1007/s11071-024-10127-7
[22] Sun B, Liu X, Wang J, Wei X, Yuan H, Dai H. Short-term performance degradation prediction of a commercial vehicle fuel cell system based on Cellular-NN and LSTM hybrid neural network. International journal of hydrogen energy, 2023, 48(23): 8613-8628. https://doi.org/10.1016/j.ijhydene.2022.12.005
[23] Zheng Q Q, Shen J W, Guan L N. Turing instability and pattern formation induced by noise in the modified SIR model. Nonlinear Dynamics, 2025, 113(5): 4355-4368. https://doi.org/10.1007/s11071-024-09927-8
[24] Rajamani K T, Rani P, Siebert H, ElagiriRamalingam R, Heinrich M P. Attention-augmented U-Net (AA-U-Net) for semantic segmentation. Signal, image and video processing, 2023, 17(4): 981-989. https://doi.org/10.1007/s11760-022-02302-3
[25] Chen H, Qin Y, Liu X, Wang H, Zhao J. An improved DeepLabv3+ lightweight network for remote-sensing image semantic segmentation. Complex & Intelligent Systems, 2024, 10(2): 2839-2849. https://doi.org/10.1007/s40747-023-01304-z
[26] An Y, Jing J, Li X, Zhang J, Bao J. An exclusive U-net for fine and crisp edge detection. Multimedia Tools and Applications, 2024, 83(18): 54657-54672. https://doi.org/10.1007/s11042-023-17706-7